



UNIVERSITÀ POLITECNICA DELLE MARCHE  
Repository ISTITUZIONALE

## Experimental Validation of an Emission Test Method for Source Stirred Reverberation Chamber

This is the peer reviewed version of the following article:

*Original*

Experimental Validation of an Emission Test Method for Source Stirred Reverberation Chamber / De Leo, A.; Cerri, G.; Russo, P.; Mariani Primiani, V.. - In: IEEE TRANSACTIONS ON ELECTROMAGNETIC COMPATIBILITY. - ISSN 0018-9375. - STAMPA. - 64:1(2022), pp. 11-18. [10.1109/TEMC.2021.3102264]

*Availability:*

This version is available at: 11566/291850 since: 2024-05-10T17:25:43Z

*Publisher:*

*Published*

DOI:10.1109/TEMC.2021.3102264

*Terms of use:*

The terms and conditions for the reuse of this version of the manuscript are specified in the publishing policy. The use of copyrighted works requires the consent of the rights' holder (author or publisher). Works made available under a Creative Commons license or a Publisher's custom-made license can be used according to the terms and conditions contained therein. See editor's website for further information and terms and conditions.

This item was downloaded from IRIS Università Politecnica delle Marche (<https://iris.univpm.it>). When citing, please refer to the published version.

(Article begins on next page)

© 2021 IEEE. Personal use of this material is permitted. Permission from IEEE must be obtained for all other uses, in any current or future media, including reprinting/republishing this material for advertising or promotional purposes, creating new collective works, for resale or redistribution to servers or lists, or reuse of any copyrighted component of this work in other works.

# Experimental Validation of an Emission Test Method for Source Stirred Reverberation Chamber

Alfredo De Leo, *Member, IEEE*, Graziano Cerri, *Member, IEEE*, Paola Russo, *Member, IEEE*, and Valter Mariani Primiani, *Senior Member, IEEE*

**Abstract** — This paper reports on the experimental validation of a method to predict radiated emissions of an equipment under test in a reverberation chamber where the multiple monopole source stirring technique is implemented. The method is validated for three different case studies: a loop, a slot in a metal enclosure and a realistic device comprised of the chassis of a power supply for a workstation. The reconstruction of the free space electromagnetic emissions starting from measurements in a reverberation chamber is compared with measurements in an anechoic environment. A statistical analysis of the uncertainty due to a positioning error of the field sample measurement points is also proposed.

**Keywords-component:** *reverberation chamber; source stirring; emission test*

## I. INTRODUCTION

THE reverberation chamber (RC) is accepted as an alternative test site in electromagnetic compatibility (EMC) testing [1]. The field stirring techniques include various mechanical methods and source stirring methods: a wide description of the most commonly used RC types and modes of stirring can be found in [2]. In particular, the source stirring methods might be achieved by varying the frequency of the source feeding the chamber, by steps larger than the coherence bandwidth, or by varying the position of the field source inside the chamber. A particular way to implement this second method, without moving anything inside the chamber, is given by the adoption of many fixed antennas, subsequently connected to the power generator (immunity test) or to the receiver (emission test). In [3], several monopoles on the chamber walls were adopted to that purpose, named multiple monopole source stirring (MMSS). Regardless of the adopted stirring techniques, emission determination by an RC is based on the measurement of the total power radiated by the equipment under test (EUT). Subsequently, by applying an estimated maximum EUT's directivity, the maximum electric field that the EUT would radiate at a certain distance (e.g. 3 m, 10 m) is determined, assuming a traditional open area test site (OATS) or a fully anechoic chamber (FAC) [4]. The EUT's maximum directivity is estimated from its dimensions and the operating frequency [5] [6] [7]. In case of an RC already operating with the MMSS, an alternative way was proposed to compute the EUT radiation in FAC (or OATS) based on the

definition of proper equivalent sources [8] [9]. Equivalent sources are derived from the electric field values sampled on the chamber walls (normal component) when the EUT is inside the working volume. The method is also able to provide the EUT emission along all space directions regardless of the EUT alignment inside the chamber, therefore without the necessity of rotating the EUT. In this paper, an experimental validation of this last method is presented, by applying it to a real MMSS chamber and considering passive EUTs having increasing complexity. Since the correlation among results achieved in different test sites is of crucial importance [10] [11] [12], a comparison with results obtained in free space is also presented, together with an analysis of the effect due to monopole positioning uncertainty on the RC walls.

This paper is organized as follows. In section II, the theoretical method, based on the recovery of equivalent sources, is briefly described. In section III, the experimental set-up is described for both RC measurements and free space validation measurements. In section IV, results are reported for three EUTs by comparing the maximum distant radiated field predicted by the RC measurement and verified in free space. In section V, the uncertainty in the radiation prediction due to monopole positioning and orientation is analyzed. Finally, a brief conclusion summarizes the achieved results.

## II. DESCRIPTION OF THE ADOPTED PROCEDURE

The procedure is based on the possibility to represent the emission of an EUT both inside a RC and in free space through the same set of equivalent sources, whose values are obtained from an opportune sampling of the electric field inside the chamber.

The detailed description of the method to obtain the equivalent sources, the demonstration of its theoretical self-consistence, the effect of the number and the position of the equivalent sources on the accuracy, the determination of their values through an iterative procedure and the convergence of the algorithm are reported in [8] and [9]. For sake of convenience, the Appendix reports a short guide that describes the use of the method and the algorithm in a real emission test.

The method has been developed to reconstruct the emissions of an EUT through the electric field values sampled inside a rectangular cavity. A MMSS RC is the most suitable structure to implement the algorithm, because it is already equipped with

monopoles that can be used for measuring the electric field emitted by an EUT, so no additional instrumentation and set-up are required.

The procedure consists of three steps: in the first, the EUT emission inside the MMSS RC is measured in a set of sampling points on the walls; in the second, the equivalent sources that generate the same EUT emission inside the RC are evaluated; in the third, the field radiated by the equivalent sources in free space is calculated and compared to measurement in an anechoic environment.

The method is based on the assumption that the power emitted by the EUT inside the RC is the same as that of the EUT in free space.

In more detail, the first step of the model consists in placing the EUT into the working volume of the RC, as is usually done in EMC testing. Then, the electric field samples sensed by the monopoles are collected and stored because they constitute the reference values. Since the antennas are mounted on the walls, only the field component orthogonal to the metallic RC surface is measured.

Subsequently, in the second step, a specifically developed algorithm generates a set of equivalent electric and magnetic currents virtually placed in the working volume.

A grid, whose points are regularly spaced by half a wavelength, is generated in the whole working volume. Three electric and three magnetic equivalent currents, oriented along the three orthogonal directions, are placed in each grid point.

These currents, called equivalent sources, are not known a priori and must represent a quite general radiating structure (the real EUT).

The values of the equivalent sources are determined by the algorithm, minimizing the difference between the theoretical field values due to the equivalent sources in the RC samples positions and the EUT reference samples measured in the first step. More details on the model and its theoretical validation can be found in [8] [9] [15].

Finally, once the equivalent sources are fixed, they are placed in free space, and their radiation can be calculated in any direction and for any distance.

In this paper, the radiation of the equivalent sources is directly compared to measurements performed in an anechoic environment.

### III. MEASUREMENT SET-UP

This section describes the experimental set-up used to compare the reconstruction of the radiated emission of an EUT placed in an RC, with the measurement of the electric field radiated by the same EUT placed into an anechoic environment.

#### A. Radiated Emission in Reverberation Chamber

The RC is a rectangular cavity, made of galvanized steel. Its dimensions are 800 mm along the x axis, 900 mm along the y axis and 1000 mm along the z axis.

The receiving monopole is sequentially inserted in the cavity through holes placed on the walls, as shown in Figure 1. On each wall, a set of 20 circular holes (radius 2.5 mm) is present,

for a total of 120 holes. Their irregular distribution is necessary to prevent unwanted effect due to symmetry [13] that could reduce the uncorrelation degree of the samples. The unused holes do not affect the quality factor of the chamber [14], and therefore do not perturb the measurement result.

The receiving monopole is a panel mount SMA female coaxial connector whose length is 19 mm covered by polytetrafluoroethylene (inset of Figure 1). The monopoles are manually inserted and held into the holes present in the RC's walls; the availability of an electronic switch can automate the measurement procedure.

The working volume of the RC is a sub region 15 cm away from each metallic wall [14].

The EUT is connected to port 1 of the VNA and the receiving antenna to port 2.

The cable that connects the EUT to the VNA crosses the walls of the RC from side to side using an N-type pass-through panel connector.

Each measurement consists in the 2-port scattering matrix measured in 1601 frequency points in the frequency range between 675 MHz and 6 GHz. The lowest frequency is three times the first resonating mode of the cavity, the highest one is limited by the VNA working frequencies.

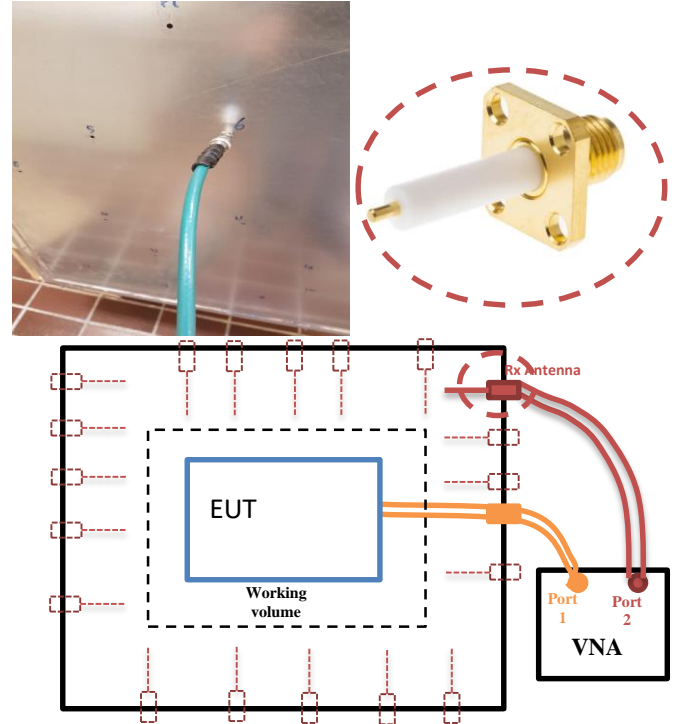


Fig. 1. Measurement setup using a MMSS RC as test site and the used monopole.

The proposed method in is used to obtain the electric field radiated in free space from the measurement of the electric field collected close to the walls using the monopoles.

The relation between  $V_{VNA}$ , the voltage measured by the VNA, and  $E_n$ , the normal component of the electric field is (1)

$$V_{VNA} = E_n l_{eff} \frac{50}{50 + Z_{ant}}, \quad (1)$$

where  $l_{eff}$  is the effective length of the monopole antenna and  $Z_{ant}$  is its impedance, that can be calculated from the measured scattering matrix, where

$$V_{VNA} = S_{21} \sqrt{50 P_{inc}} \quad (2)$$

For all the measurements reported in this paper, the output power ( $P_{inc}$ ) of the VNA was set to 0 dBm.

#### B. Radiated Emission in an Anechoic Environment

The EUT radiated emissions were measured in an anechoic environment (AE), as shown in Figure 2: the EUT was placed on a rotating platform and connected to port 2 of the VNA.

The receiving antenna was a double ridge horn antenna, well matched in the whole explored frequency range, and connected to port 1 of the VNA. A time domain approach was chosen to carry out the measurements. The time gating utility of the VNA was used to isolate the pulse radiated directly from the EUT from the residual reflections due to the environment.

The distance between the EUT and the receiving antenna is 2.3 m, smaller than the standard prescription of 3 m due to the environment dimension and length constraints of the cables. However, at this distance, the far field condition is fulfilled in the whole analyzed frequency range.

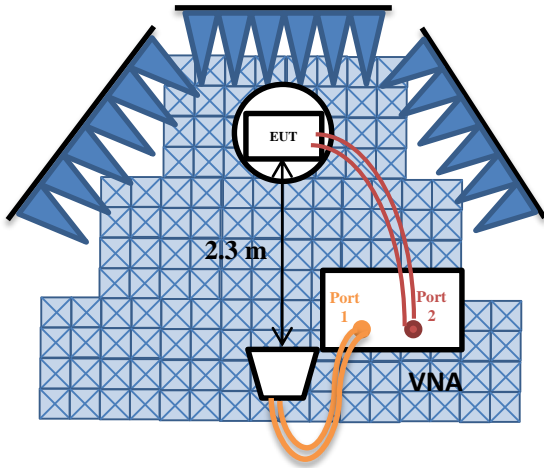


Fig. 2. Measurement setup using an anechoic corner as test site: the absorbing panels are placed on the floor and vertical walls.

### IV. EXPERIMENTAL VALIDATION OF THE METHOD

This section reports on the comparison between the radiated emissions measured in free space and the corresponding values indirectly calculated from the knowledge of the electric field close to the walls inside the RC.

Three case studies are reported: a circular loop, a slot on a metallic box and a realistic EUT consisting of a chassis of a power supply for a workstation. Three frequencies ( $f_1 = 1$  GHz,

$f_2 = 2$  GHz and  $f_3 = 3$  GHz) were chosen in the range  $675 \text{ MHz} \leq f \leq 6 \text{ GHz}$  to explore all the RC stirring conditions.

In particular, from RC dimensions, the resonating frequency of the first eigenmode is 225 MHz ( $f_0$ ). As it is generally accepted, for frequencies lower than  $6f_0$  the RC is undermoded, so the first frequency was chosen in this region.

After performing some measurements as shown in [14] and [16], it results that at 3 GHz our RC is well stirred, so the third frequency chosen belongs to the overmoded region. Finally, the second frequency was chosen as an intermediate frequency.

Subsection A reports on the typical result of an emission test: the comparison between the maximum radiated emission measured in the AE and that retrieved from measurements in the RC.

Subsection B reports on some examples of the spatial emission reconstruction in the most significant planes, used for identifying the direction where the electric field assumes the maximum value.

#### A. Measurement of the Maximum Emissions Value

In this first case study, the EUT is a near field probe, characterized by a circular loop having an outer diameter of 6 cm (Figure 3).

The loop is placed at the center of the working volume of the RC with the loop axis parallel to the z direction and the stick of the probe parallel to the y axis.

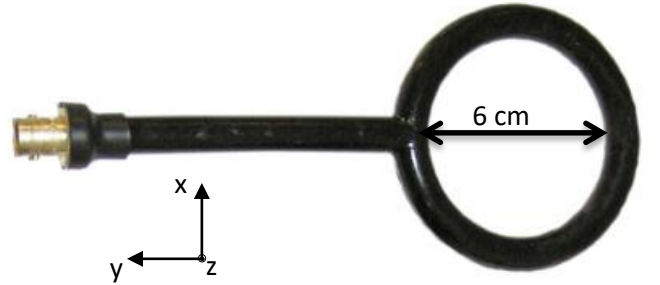


Fig. 3. The loop used in the emission measurement as radiating EUT.

In the second case study, the EUT is a metallic box having dimensions  $90 \text{ mm} \times 100 \text{ mm} \times 200 \text{ mm}$  (Figure 4). In the wider face, a rectangular slot ( $75 \text{ mm} \times 2 \text{ mm}$ ) was opened and in the orthogonal face, an SMA pass-through connector was inserted to feed a folded monopole placed inside the box. The folded monopole has a L shape, one side is parallel to the z-axis and the other side to the x-axis, both are 20 mm long.



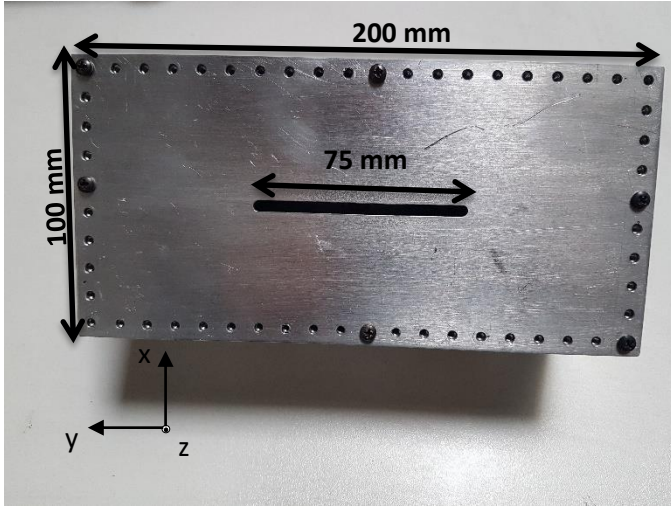
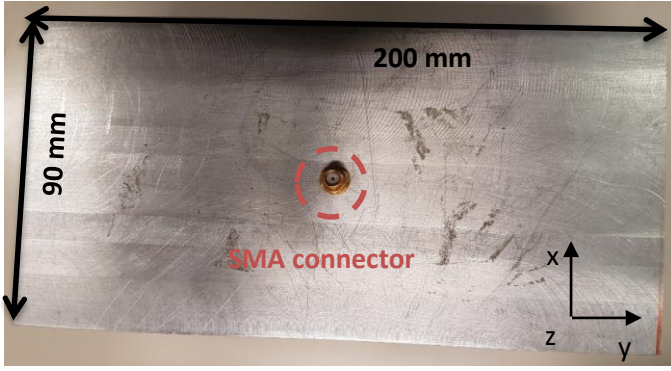


Fig. 4. The slot on the metallic box and its dimension.

The third case study represents a real commercial device. It is the chassis of a power supply (Figure 5) having an internal transmitting circuit, plugged using an N-type connector to simulate the common mode radiation of a PBC board.

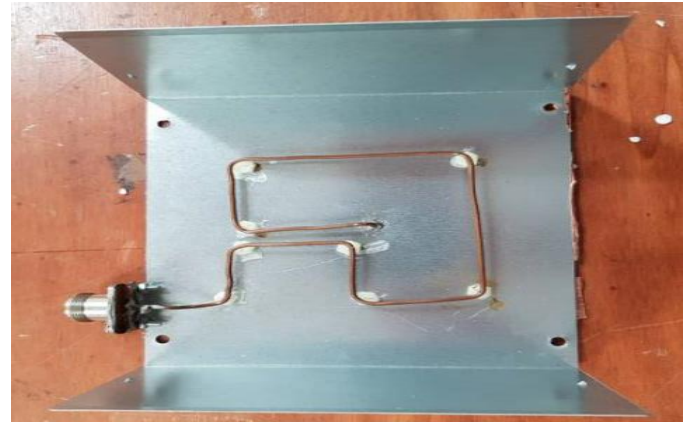
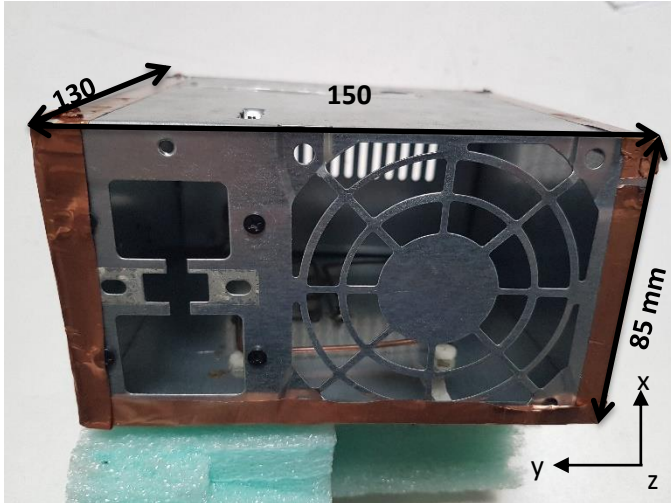


Fig. 5. The chassis of a power supply of a workstation (up) and the transmitting circuit (down).

Table I reports the comparison between AE measurements and the reconstructed values: the maximum values of the total electric field are reported.

TABLE I - RADIATED EMISSIONS: MAXIMUM VALUES OVER THE SCANNED PLANES

EUT	Freq. [GHz]	Electric Field at 2.3 m [mV/m]	
		AE meas.	RC meas.
Loop (planes $\phi=0$ and $\theta=\pi/2$ )	1	1.8	1.9
	2	2.9	2.8
	3	5.3	5.6
Slot (planes $\phi=0$ and $\phi=\pi/2$ )	1	82.9	84.6
	2	74.6	77.0
	3	32.9	36.1
Power Supply (planes $\phi=0$ and $\phi=\pi/2$ )	1	26.6	28.6
	2	32.9	33.8
	3	37.8	38.4

It is well evident that the proposed method is very accurate also in the case of a complex object whose dimensions are comparable with wavelength.

#### B. Determination of the Emission in the Space

This subsection presents further results related to the radiation emission reconstruction of the same EUTs of the previous subsection.

Even though the proposed method is not intended for antenna radiation pattern measurements inside an RC, the ability of the algorithm to explore the 3D emission is crucial for obtaining the maximum radiated field of the EUT considering all space directions. For practical reasons, only emissions in the principal planes are reported.

Figure 6 shows the emission of the loop. In particular, the red pattern represents the experimental electric field measured in the AE, whereas the blue line describes the field pattern retrieved from field sampling on the RC walls. The capability of the method to reconstruct the emission in all directions of the

space can be appreciated, as well as its quite satisfactory accuracy. In Figure 6, with reference to the coordinates system reported in Figure 3, the planes  $\phi = 0$  and  $\theta = \pi/2$  are reported.

Due to the field sampling technique, (40 monopoles for each direction), and the quasi-cubic geometry of the structure, we assume that inside the RC there are no preferential planes in observing the EUT emissions. Therefore, it is not expected that the algorithm has different level of accuracy in the evaluation of the EUT emission when considering different planes.

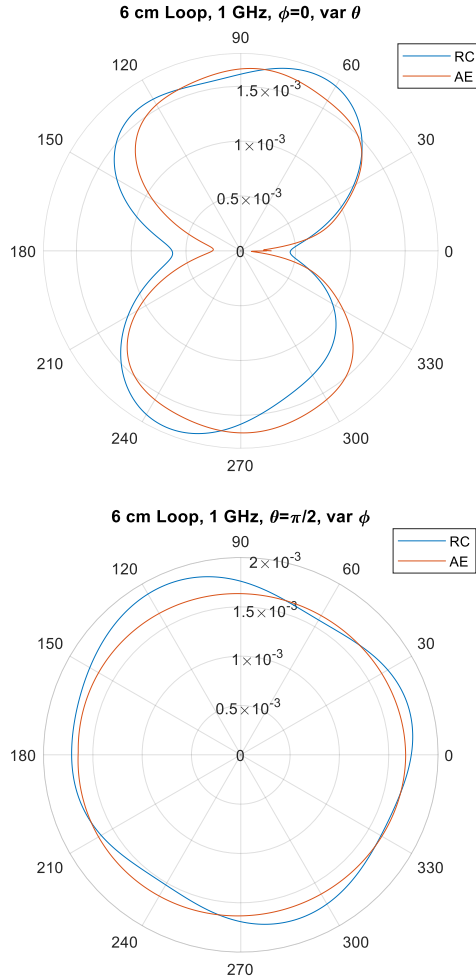


Fig. 6. Radiated emissions of a loop having 6 cm of diameter measured at 1 GHz at the distance of 2.3 m: comparison between measurements in RC (blue) and AE environment (red). Planes  $\phi=0$ , (up) and  $\theta=\pi/2$  (down) are shown. The unit of the reported results is [V/m].

The good level of prediction is confirmed also for different EUTs and when varying the frequency. As regards the slot in the metallic chassis, Figure 7 shows the capability of the method for providing information about the directional properties of the radiating structure, that exhibits the maximum emission in the direction ( $\theta = 0$ ), and negligible radiation in the opposite direction.

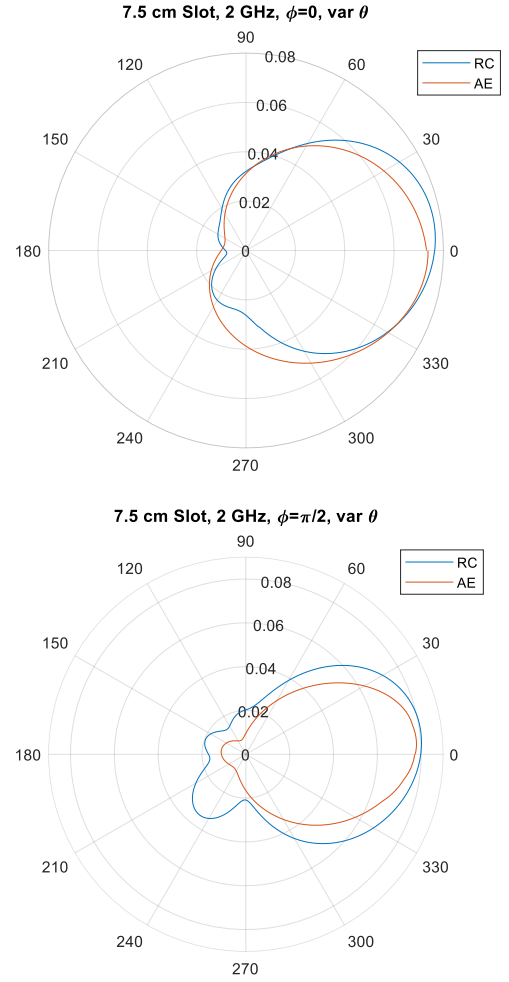


Fig. 7. Radiated emissions of a metallic box having a 7.5 cm slot, measured at 2 GHz at the distance of 2.3 m: comparison between measurements in RC (red) and AE environment (blue). Planes  $\phi=0$ , (up) and  $\phi=\pi/2$  (down) are shown. The unit of the reported results is [V/m]

It is interesting to observe that, due to the finite dimensions of the aperture plane, a considerable emission occurs also in the lateral direction ( $\theta = \pi/2$ ).

Finally, the third case study was implemented to test the algorithm in a realistic situation and to stress the method with a complex object: the chassis of the power supply, as shown in Figure 5, has many apertures that are comparable to the wavelength at the frequency of 3 GHz with different dimensions, shapes and orientations.

For this reason, the radiated emissions along different spatial directions (Figure 8) are irregular and exhibit many lobes. In this case, the reconstruction of the single lobe is less accurate than in the previous cases, however, the measured pattern envelops the estimated one, and moreover, the space regions with the higher emission are correctly predicted.

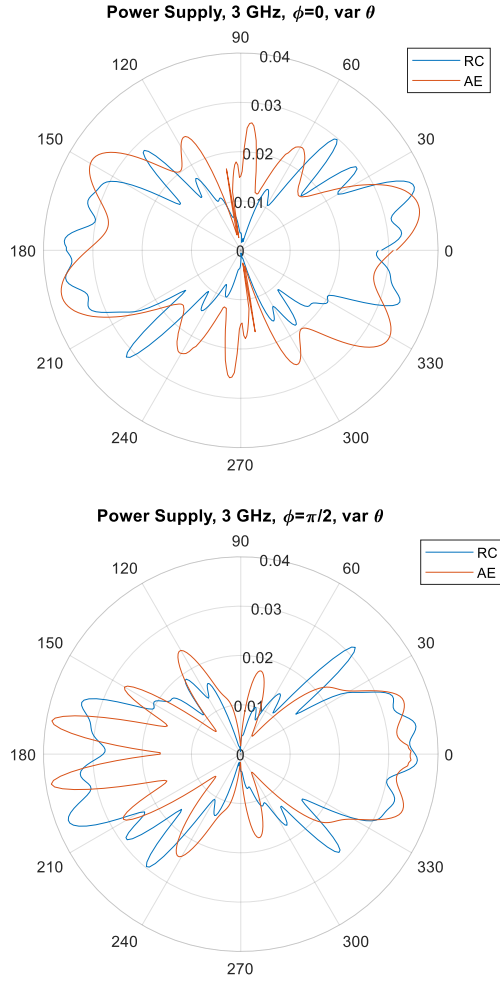


Fig. 8. Radiated emissions of a chassis of a power supply, measured at 3 GHz at the distance of 2.3 m: comparison between measurements in RC (blue) and AE environment (red). Planes  $\phi=0$ , (up) and  $\phi=\pi/2$  (down) are shown. The unit of the reported results is [V/m]

## V. ANALYSIS OF THE EFFECT OF THE MEASUREMENT UNCERTAINTY

In this section, the effect of experimental uncertainty on the reconstruction of radiated emission based on the samples of the electric field inside an RC is explored.

Two causes of uncertainty mainly affect this experimental setup: the uncertainty of the exact position of the monopole that senses the field and the uncertainty of its direction.

The uncertainty of the position of a hole centered in  $(x_0, y_0)$  and having diameter  $d = 5$  mm can be assumed having a rectangular distribution in the intervals  $[x_0-d/2, x_0+d/2]$  for the coordinate  $x$  and  $[y_0-d/2, y_0+d/2]$  for the coordinate  $y$ .

Supposing  $\theta = 0^\circ$  the ideal direction of the monopole, orthogonal to the wall of the RC, it can be assumed that also this parameter could have a rectangular distribution in the interval  $[-10^\circ, 10^\circ]$ .

A rectangular distribution has been considered for both uncertainties because they are due to the uncertainty of a measurement procedure, concerning the coordinates of the hole

center the first case, and the alignment of the monopole in the second one. Being the contributions of these two uncertainties statistically independent, their combined distribution can be assumed as a normal function. So, for a confidence level of 95%, the interval bounded between  $(\mu_{RC} - 2\sigma_{RC})$  and  $(\mu_{RC} + 2\sigma_{RC})$  is considered.

The propagation of these two uncertainties on the reconstruction of the radiated emission has been explored using the analytical model [8] that allows to take into account both parameters.

Table II reports the results of 100 simulations, obtained by randomly varying the coordinates of all the sample points and monopole directions in the above-mentioned uncertainty ranges. The mean values  $(\mu_{RC})$  and the standard deviations  $(\sigma_{RC})$  are computed for each direction of the 3D emission of each EUT.

It can be appreciated that the maximum values of the radiated emissions measured in free space ( $AE_{MAX}$ ) are bounded between  $(\mu_{RC} - 2\sigma_{RC})_{MAX}$  and the  $(\mu_{RC} + 2\sigma_{RC})_{MAX}$

TABLE II – UNCERTAINTY EFFECT ON RADIATED EMISSIONS OVER THE SCANNED PLANES

EUT	Freq. [GHz]	Electric Field at 2.3 m [mV/m]		
		$(\mu_{RC} + 2\sigma_{RC})_{MAX}$	$(\mu_{RC} - 2\sigma_{RC})_{MAX}$	$AE_{MAX}$
Loop (planes $\phi=0$ and $\theta=\pi/2$ )	1	2.1	1.7	1.9
	2	3.1	2.6	2.8
	3	5.9	5.1	5.6
Slot (planes $\phi=0$ and $\phi=\pi/2$ )	1	96.1	65.4	84.6
	2	87.8	61.8	77.0
	3	40.2	30.1	36.1
Power Supply (planes $\phi=0$ and $\phi=\pi/2$ )	1	33.4	24.6	28.6
	2	37.1	31.2	33.8
	3	48.7	26.2	38.4

Figure 9 shows the radiation of the loop measured in AE (red line), compared to  $(\mu_{RC} - 2\sigma_{RC})_{MAX}$  and  $(\mu_{RC} + 2\sigma_{RC})_{MAX}$  values (dashed and dotted blue lines, respectively). It can be noticed that AE emissions are reconstructed in an acceptable way over most of the directions in the considered planes, especially where the EUT radiation is higher.



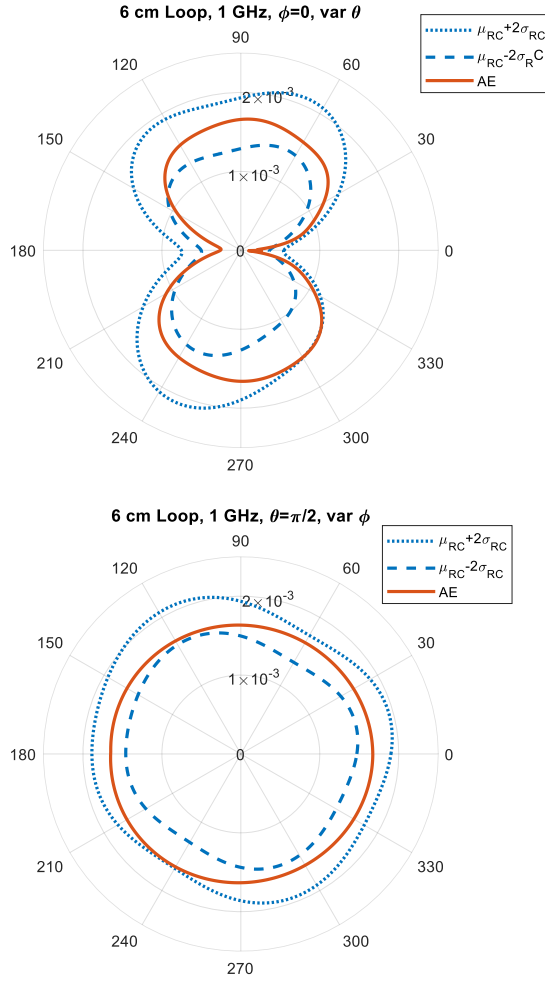


Fig. 9. Effect of an uncertainty on the radiated emission of a 6 cm loop, due to an uncertainty of 2.5 mm on the position of the monopoles and  $10^\circ$  on their direction. Planes  $\phi=0$ , (up) and  $\theta=\pi/2$  (down) are shown. The unit of the reported results is [V/m]

As regards the slot (Figure 10), also in this case study, the uncertainty analysis returns values of electromagnetic radiation that almost includes the AE measurements in the interval of prediction  $(\mu_{RC} \pm 2\sigma_{RC})_{MAX}$ .

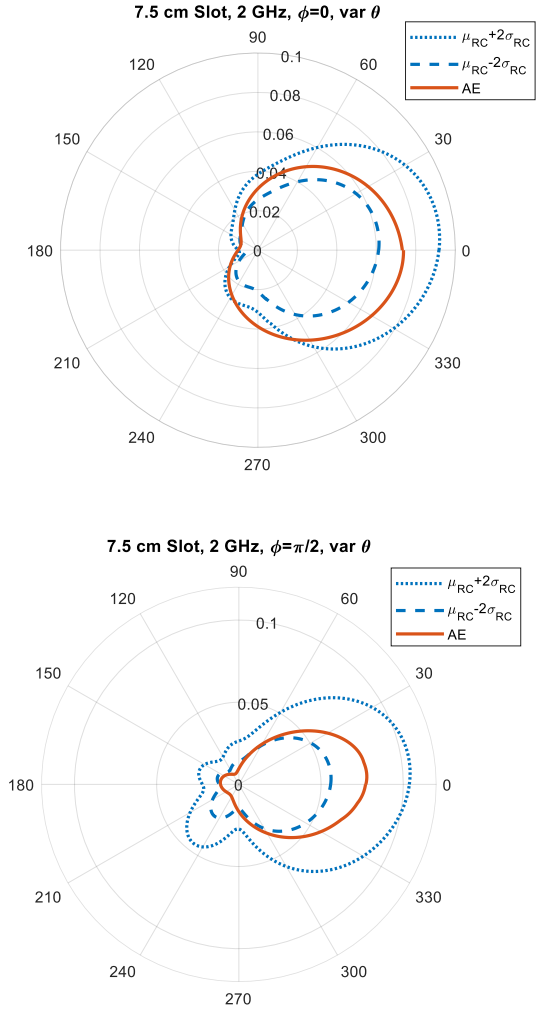


Fig. 10. Effect of an uncertainty on the radiated emission of a 7.5 cm slot on a metallic box, due to an uncertainty of 5 mm on the position and  $10^\circ$  on the direction of the electric field samples on the RC walls. Planes  $\phi=0$ , (up) and  $\phi=\pi/2$  (down) are shown. The unit of the reported results is [V/m]

Finally, from the uncertainty analysis on the emission of the EUT made by the chassis of the power supply, it emerges (Figure 11) that the effect is greater than in the other two case studies. It is due to the fact that at 3 GHz, the uncertainty of  $\pm 2.5$  mm on the position becomes greater in terms of wavelength.

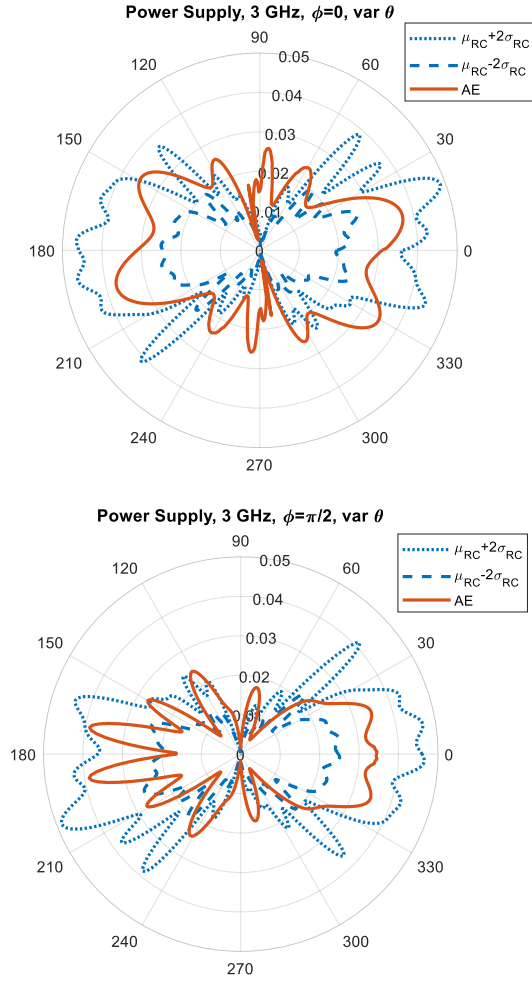


Fig. 11. Effect of an uncertainty on the radiated emission of a chassis of a power supply, due to an uncertainty of 5 mm on the position and  $10^\circ$  on the direction of the electric field samples on the RC walls. Planes  $\phi=0$ , (up) and  $\phi=\pi/2$  (down) are shown. The unit of the reported results is [V/m]

## VI. CONCLUSIONS

The work presents the experimental validation of a method to predict radiated emission starting from electric field samples collected on the walls of an RC equipped for the MMSS technique.

Three different EUTs are considered, at three different frequencies, and the measurements confirm the capability of the method to reconstruct the radiated emissions.

It means that the maximum value of the electric field is detected over all the directions, and the comparison with the measurements in an anechoic environment have a good level of agreement.

The analysis on the effect of the uncertainty of the position and the direction of the monopole was successfully performed, and it emerges that the maximum value of the radiated emission measured in the anechoic environment is bounded into the uncertainty range predicted by the model.

All the results are satisfactory and encourage research activity to be developed.

The next step of the research activity would be the extension of the method in order to reconstruct the emissions from the absolute values of the electric samples, so that a spectrum analyzer, or an EMI receiver, will be used instead of the VNA. In a general scenario, in fact, the phase correlation between the EUT and the field samples might not be available.

The achieved results also confirm that the initial assumption of comparable emission of the EUT in the RC and in free space, is acceptable for the analyzed situations (general, practical and lossless EUTs) and for the investigated frequency range (lowest frequency equal to 4.4 times the chamber fundamental mode resonance). In other cases, the chamber loading on the EUT might be heavier, especially at even lower frequencies. Future activities will be devoted to analyze this aspect.

## REFERENCES

- [1] Reverberation Chamber Test Methods, International Electrotechnical Commission (IEC), Std. 61 000-4-21, 2011.
- [2] R. Serra et al., "Reverberation chambers a la carte: An overview of the different mode-stirring techniques," in *IEEE Electromagnetic Compatibility Magazine*, vol. 6, no. 1, pp. 63-78, First Quarter 2017, doi: 10.1109/MEMC.2017.7931986.
- [3] A. De Leo, V. M. Primiani, P. Russo and G. Cerri, "Low-Frequency Theoretical Analysis of a Source-Stirred Reverberation Chamber," in *IEEE Transactions on Electromagnetic Compatibility*, vol. 59, no. 2, pp. 315-324, April 2017, doi: 10.1109/TEMC.2016.2613402.
- [4] F. B. J. Leferink, D. J. Groot-Boerle and B. R. M. Puylaert, "OATS emission data compared with free space emission data," *Proceedings of International Symposium on Electromagnetic Compatibility*, Atlanta, GA, USA, 1995, pp. 333-337, doi: 10.1109/ISEMC.1995.523575.
- [5] G. Koepke, D. Hill and J. Ladbury, "Directivity of the test device in EMC measurements," *IEEE International Symposium on Electromagnetic Compatibility. Symposium Record (Cat. No.00CH37016)*, Washington, DC, 2000, pp. 535-539 vol.2, doi: 10.1109/ISEMC.2000.874677.
- [6] H. Garbe and S. Battermann, "Converting total-radiated-power measurements to equivalent E-Field Data," *2008 IEEE International Symposium on Electromagnetic Compatibility*, Detroit, MI, 2008, pp. 1-6, doi: 10.1109/ISEMC.2008.4652048.
- [7] P. Wilson, "Radiation Patterns of Unintentional Antennas: Estimates, Simulations, and Measurements," in *Proc. Asia-Pacific Symp. Electromagn. Compat.*, Apr. 2010, pp. 985-989.
- [8] A. De Leo, G. Cerri, P. Russo and V. Mariani Primiani, "A Novel Emission Test Method for Multiple Monopole Source Stirred Reverberation Chambers," in *IEEE Transactions on Electromagnetic Compatibility*, vol. 62, no. 5, pp. 2334-2337, Oct. 2020, doi: 10.1109/TEMC.2020.2999651.
- [9] De Leo, A., Cerri, G., Russo, P., Mariani Primiani, V., "A general method for radiated emission prediction in a multiple monopole source stirred reverberation chamber," (2021) *IET Science, Measurement and Technology*, DOI: 10.1049/smt2.12060
- [10] H. G. Krauthausser, "Statistical Analysis of the Correlation of Emission Limits for Established and Alternative Test Sites," in *IEEE Transactions on Electromagnetic Compatibility*, vol. 53, no. 4, pp. 863-875, Nov. 2011, doi: 10.1109/TEMC.2010.2102764.
- [11] B. Menssen, H. Brech and H. Garbe, "Measurement Validation for the Extension of Emission Measurements in Alternative Test Sites Above 1 GHz," in *IEEE Transactions on Electromagnetic Compatibility*, vol. 58, no. 4, pp. 1274-1281, Aug. 2016, doi: 10.1109/TEMC.2016.2554463.
- [12] CISPR TR 16-4-5:2006+AMD1:2014 CSV Consolidated version. "Specification for radio disturbance and immunity measuring apparatus and methods - Part 4-5: Uncertainties, statistics and limit modelling - Conditions for the use of alternative test methods"
- [13] A. De Leo, G. Cerri, P. Russo and V. M. Primiani, "Theoretical Radiated Emission Prediction of an Aperture Array by Reverberation Chamber

Field Sampling," 2020 International Symposium on Electromagnetic Compatibility - EMC EUROPE, Rome, Italy, 2020, pp. 1-6, doi: 10.1109/EMCEUROPE48519.2020.9245853.

- [14] A. D. Leo, G. Cerri, P. Russo and V. M. Primiani, "Experimental Validation of an Analytical Model for the Design of Source-Stirred Chambers," in IEEE Transactions on Electromagnetic Compatibility, vol. 60, no. 2, pp. 540-543, April 2018, doi: 10.1109/TEMC.2017.2723804.
- [15] A. De Leo, G. Cerri, P. Russo and V. M. Primiani, "Statistical Analysis of the Induced Voltage on a DUT in a Reverberation Chamber where Mechanical and Source Stirring Actions are Implemented," 2019 International Symposium on Electromagnetic Compatibility - EMC EUROPE, Barcelona, Spain, 2019, pp. 241-246, doi: 10.1109/EMCEurope.2019.8871820.
- [16] A. De Leo, G. Andrieu and V. M. Primiani, "'Well-Stirred' Condition Method applied to a Multiple Monopole Source Stirred Reverberation Chamber," 2020 International Symposium on Electromagnetic Compatibility - EMC EUROPE, 2020, pp. 1-5, doi: 10.1109/EMCEUROPE48519.2020.9245821.

## APPENDIX

In this appendix the procedure based on the theoretical model described in [8] [9] [15], is briefly reported, and aimed at applying the algorithm to the situation of a real emission test.

The reference scenario is a rectangular cavity with metallic walls. Inside, an EUT radiates electromagnetic power and the electric field is measured in  $N_s$  sampling points on the walls, so only the normal component is considered. The electric field samples radiated by the EUT constitute the measured reference set ( $E_n^{ref}$ ,  $n = 1, \dots, N_e$ ), that is stored, and provided to the algorithm for the emission estimation. Another measurement required by the algorithm concerns the size and the position inside the cavity of a sub-volume containing the EUT, called equivalent source volume (ESV). The ESV can be the whole working volume, or a sub-volume of its.

Using these geometrical data, the algorithm defines preliminarily a regular grid of points in the ESV, where  $N_{eq}$  equivalent sources  $\vec{S}_i^{eq}$  ( $\vec{S}_i^{eq} = \vec{J}_i^{eq}$ , or  $\vec{S}_i^{eq} = \vec{M}_i^{eq}$ ,  $i = 1, \dots, N_{eq}$ ) are placed. In [9] it is demonstrated that the optimal choice is to space these points by half a wavelength. In each point, three magnetic and three electric equivalent currents, having orthogonal directions, are positioned. These points can be chosen on the surface of the ESV, or in its whole volume, but, if the radiation mechanism of EUT is a priori known, for example after a visual inspection, a great advantage in terms of algorithm efficiency can be achieved with an "ad hoc" location of the equivalent sources.

After this preliminary setup, the algorithm can start the iterative procedure aimed at computing the value of the equivalent currents, and, in particular, at each iteration the value of only one current is determined. First, the electric field  $E_n^{eq}(\vec{S}_{i^*}^{eq})$  due to each equivalent current is reconstructed by the algorithm in correspondence of all the sampling points, and the distance  $d_i$  between the reference field and reconstructed values is evaluated according to (A.1)

$$d_i = \frac{\sum_{n=1}^{N_s} |E_n^{ref} - E_n^{eq}(\vec{S}_{i^*}^{eq})|}{\sum_{n=1}^{N_s} |E_n^{ref}|}, \quad i = 1, \dots, N_{eq} \quad (A.1)$$

The  $i^*$ -th equivalent current  $\vec{S}_{i^*}^{eq}$  that minimizes  $d_i$  among all the equivalent sources is found and fixed.

Then the residual field is computed according to (A.2).

$$E_n^{res} = E_n^{ref} - E_n^{eq}(\vec{S}_{i^*}^{eq}), \quad n = 1, \dots, N_s \quad (A.2)$$

Next iterations follow the same procedure from (A.1), assuming at the  $k$ -th iteration the reference values equal to the residual field related to the previous iteration (A.3).

$$(E_n^{ref})^k = (E_n^{res})^{k-1}, \quad n = 1, \dots, N_s, \quad k = 1, \dots, N_{iter} \quad (A.3)$$

so that in each step the equivalent current that best fits the residual field is found.

The iterations are stopped when the desired accuracy in the reconstruction of the samples is reached.

Finally, once all equivalent sources have been determined, the algorithm regards them as if they were in free space, their radiation is computed in all directions, the maximum emission found, and then compared with the emission limits provided by the standard. In the current paper, the radiation of the equivalent sources in free space has been compared with measurements in AE.